NASA Technical Paper 2428

April 1985

NASA-TP-2428 19850014926

Characteristic Vector Analysis of Inflection Ratio Spectra: New Technique for Analysis of Ocean Color Data

Gary W. Grew

NASA

NASA Technical Paper 2428

1985

Characteristic Vector Analysis of Inflection Ratio Spectra: New Technique for Analysis of Ocean Color Data

Gary W. Grew

Langley Research Center
Hampton, Virginia

National Aeronautics and Space Administration

Scientific and Technical Information Branch

Abstract

Characteristic vector analysis applied to inflection ratio spectra is a promising new approach to analyzing spectral data. The technique applied to remote data collected with the Multichannel Ocean Color Sensor (MOCS), a passive sensor, appears to simultaneously map the distribution of two different phytopigments, chlorophyll *a* and phycoerythrin, in the ocean. The data set presented was from a series of warm core ring missions conducted during 1982. The data are shown to compare favorably with a theoretical model and with data collected on the same mission by an active sensor, the Airborne Oceanographic Lidar (AOL).

Introduction

Any set of spectral data, whether it is measured *in situ* or remotely sensed, may contain spectral variations caused by extraneous environmental factors. When investigators attempt to correlate these data sets with some parameter of interest, the extraneous variations can obscure the analyses. A technique is often needed for removing these factors before the analysis can be continued productively. For spectral data remotely sensed from aircraft and satellites, whether they are atmospheric, terrestrial, or oceanic data, the extraneous factors can be numerous.

Although the technique presented in this paper is applicable to other types of spectral data, it was the outcome of a search to find an algorithm to monitor chlorophyll *a* concentration in the ocean by using remotely sensed ocean color data (refs. 1 and 2). In this case, the extraneous factors are numerous, e.g., solar elevation, aerosols, air and water molecules, sea state, sediments, and the ocean floor. The task of stripping away these factors has been a formidable challenge to remotely sensing chlorophyll *a* concentrations.

An algorithm which is fairly independent of the environment has recently been demonstrated to be a valuable tool in real-time measurements of chlorophyll *a* (ref. 2). The algorithm resulted from analysis of data collected with the Multichannel Ocean Color Sensor (MOCS). This passive instrument is a very stable imaging spectroradiometer which performs multispectral scanning electronically by means of an image dissector (ref. 3). It covers the visible region of the spectrum (400–700 nm) in 20 adjacent bands (tables I and II).

This chlorophyll *a* algorithm agrees remarkably well with data collected by a completely different type of instrument, the Airborne Oceanographic Lidar (AOL).

The AOL system detects laser-induced fluorescence from both chlorophyll *a* and phycoerythrin pigments of phytoplankton by using a single laser excitation wavelength (ref. 4). In a series of missions flown as part of the Nantucket Shoals Experiment in 1981 and the Warm Core Ring Experiments in 1982 (refs. 5–7), ocean spectral data were simultaneously collected by the MOCS and the AOL aboard the NASA Wallops P-3 airplane. In many cases the data correlated quite well. In other cases, however, differences occurred. In an attempt to explain these differences, the characteristic vector analysis method was applied to the MOCS data sets. In the past this type of analysis has been tried on raw MOCS data with partial success (refs. 8 and 9). In the new approach reported here, vector analysis was performed on MOCS inflection ratio spectra with much greater success.

The author wishes to thank Frank Hoge and Bob Swift of the AOL team at the NASA Wallops Flight Facility for use of their data and Janet W. Campbell of the Bigelow Laboratory for Ocean Sciences for supplying data from the Smith and Baker model.

Symbols and Abbreviations

AOL	Airborne Oceanographic Lidar
a_i	scalar multiple of ith vector
C	chlorophyll *a* concentration, μg/L
$G_{j,m}$	inflection ratio algorithm derived from signals of MOCS bands $j,\ j-m,\ j+m$
$G_{j,m,n}$	inflection ratio algorithm derived from signals of MOCS bands $j,\ j-m,\ j+n$
$H_{j,m}$	inflection ratio algorithm derived by normalizing by mean spectrum $\bar{x}_j$
$\mathbf{I}$	identity matrix
j	MOCS spectral band
ℓ_i	fractional variance of ith vector
MOCS	Multichannel Ocean Color Sensor
m	integer constant
N	number of spectra
n	integer constant
$\mathbf{P}$	difference matrix
$\mathbf{P}'$	transpose of difference matrix
r	correlation coefficient
$\mathbf{S}$	variance-covariance matrix

$S_j, S_{j\pm m}, S_{j+n}$	MOCS signal for bands j, $j \pm m$, and $j + n$, respectively
$\mathbf{V}_i$	ith characteristic vector
$\mathbf{X}$	data matrix
x_j	magnitude of band j of spectrum
λ_i	characteristic root of ith vector

Algorithm

The general form of the algorithm is given by

$$G_{j,m,n} = \frac{S_j^2}{S_{j-m}S_{j+n}} \tag{1}$$

where S_j is the MOCS signal for band j, and m and n are constants. This algorithm, which amplifies and monitors changes in the spectral features, has been labeled the "inflection ratio algorithm" (ref. 2).

As a first step toward simplifying the analyses, all forms of the $G_{j,m,n}$ algorithm in which $m = n$, or

$$G_{j,m} = \frac{S_j^2}{S_{j-m}S_{j+m}} \tag{2}$$

were investigated. Subsequently, as a further simplification, all possible values of this algorithm for $m = 2$, or

$$G_{j,2} = \frac{S_j^2}{S_{j-2}S_{j+2}} \qquad (j = 3 \text{ to } 18) \tag{3}$$

were investigated because (1) the smaller of the value of m, the less the influence of the environment on the algorithm, and (2) the spectral features of interest are about 60 nm wide (four MOCS channels at a bandwidth of 15 nm per channel). An independent analysis of the algorithm can be found in reference 10.

For $j = 7$ in equation (3), the algorithm has been found to correlate quite well with chlorophyll a. Thus,

$$G_{7,2} = \frac{S_7^2}{S_5 S_9} = \frac{(S_{490\text{ nm}})^2}{(S_{460\text{ nm}})(S_{521\text{ nm}})} \tag{4}$$

By using calibrated AOL data from one particular mission over Nantucket Shoals on May 9, 1981 (ref. 2), the linear regression equation

$$\ln C = 10.19 - 7.33G_{7,2} \tag{5}$$

was derived, where C is the chlorophyll a concentration in μg/L. This data set, shown in figure 1, has a correlation coefficient of 0.985. The equation was used successfully during the Nantucket Shoals Experiment and, a year later, during the Warm Core Ring Experiments. The approximate flight paths of two examples are shown in figure 2. Simultaneous measurements of chlorophyll a made by MOCS and AOL on May 14, 1981, are compared in figure 3 with ship data along a track south of the Shoals. Figure 4 shows MOCS and AOL data collected on April 30, 1982, during a Warm Core Ring mission. No ship data were available during this flight. By inspection, the correlations between MOCS and AOL data are good in both figures 3 and 4. Other flights show similar results.

Differences do occur, however, and a mission in which the differences were obvious occurred on June 24, 1982. On this flight, a star pattern was flown over warm core ring 82-B, as shown in figure 5. Figure 6 contains plots of AOL and MOCS data collected along line #6A of the star. The variations in the measurements of chlorophyll a made by both systems show similarities and differences. Linear regression of the two chlorophyll a measurements yielded a correlation coefficient of 0.523. The plot of the MOCS data indicates the presence of two large patches, designated patch #1 and patch #2, with a lower concentration in between, whereas the plot of the AOL data shows a general rise with two smaller drops in concentration. Note that the AOL phycoerythrin feature corresponds with patch #1 of the MOCS data. To gain insight into the significance of these differences, the inflection ratio algorithm is first applied to theoretical data from Smith and Baker (ref. 11). The results are then compared with the flight data obtained on June 24.

Algorithm on Theoretical Data

Smith and Baker (ref. 11) generated a model of irradiance reflectance, $R(\lambda)$, as a function of chlorophyll-like pigments in the ocean. The symbol $R(\lambda)$ is defined as the upwelling irradiance normalized by the downwelling irradiance just below the ocean surface. Spectral curves from the model for chlorophyll concentrations between 0 and 10 μg/L are shown in figure 7. In figure 8, the algorithm $G_{j,2}$ was computed by first integrating the data in figure 7 to yield 20 spectral points (resolution of 15 nm) corresponding to the MOCS bands (table II). For comparisons with flight data, all spectra generated by applying the $G_{j,2}$ algorithm to the Smith and Baker model were normalized by the 0.0 μg/L spectrum; the results, $H_{j,2}$, are shown in figure 9. To relate these spectra to the ocean environment, the negative curvature features centered at bands 7 and 15 are associated with the absorption of light, whereas the positive curvature features centered at bands 9 and 12 are associated with the scattering of light. The absorption feature at band 7 is used in

equation (5) in estimating chlorophyll a concentrations. Note the saturation effects of the spectra above 3 μg/L in the central (green) bands. Another interesting variation is the reversal of the feature at band 15. The feature increases with increasing chlorophyll a concentration until 1 μg/L is reached, then it decreases. This reversal, observed in many MOCS data sets, is believed to occur as the backscattered light from high algae concentrations just below the ocean surface becomes stronger than the extinction of light by water molecules.

Comparison With Flight Data

From the MOCS data collected at an altitude of 150 m on June 24, 1982, $G_{j,2}$ was computed on a sample spectrum with a chlorophyll a estimate of 0.66 μg/L from each of the two patches in figure 6. These data were then normalized by a $G_{j,2}$ spectrum with a chlorophyll a estimate of 0.13 μg/L, the lowest value for this data set, collected at the start of line 6; the results are plotted in figure 10. In the figure the inflection ratio spectrum for patch #2 has a similar shape to those of the theoretical spectra (fig. 9), whereas the patch #1 spectrum is quite different—especially at the longer wavelengths. This result suggests at least one possible explanation; that is, there may be two distinctly different types of algae along this flight path—one type in patch #2, and one or both types in patch #1. This idea is reinforced by the fact that the AOL phycoerythrin estimates were higher for patch #1 than for patch #2. The next investigative step requires a means of separating these algae pigments. Characteristic vector analysis of inflection ratio spectra provides a means.

Characteristic Vector Analysis

The mathematical treatment of characteristic vector analysis can be found in a number of textbooks (e.g., refs. 12 and 13). Simonds (ref. 14) presents a good demonstration of the method of generating characteristic vectors, or eigenvectors, by carrying a set of data step-by-step through the procedure. Simonds defines the technique as "a method of examining a number of sets of multivariate response data and determining linear transformations of the data to a smaller number of parameters which contain essentially all the information in the original data." To illustrate this statement and to outline the procedure using multivariate data, consider MOCS spectra consisting of 20 spectral bands.

A set of N MOCS spectra can be written in matrix form

$$\mathbf{X} = \begin{bmatrix} x_{1,1} & \cdots & x_{1,20} \\ \cdots & \cdots & \cdots \\ x_{N,1} & \cdots & x_{N,20} \end{bmatrix} \tag{6}$$

where $x_{N,20}$, for example, is the magnitude of band 20 for spectrum N. The mean spectrum for the data set is

$$\bar{\mathbf{X}} = \{\bar{x}_1 \quad \cdots \quad \bar{x}_j \quad \cdots \quad \bar{x}_{20}\} \tag{7}$$

Subtracting the mean spectrum from each spectrum of the data set, we have

$$\mathbf{P} = \begin{bmatrix} x_{1,1} - \bar{x}_1 & \cdots & x_{1,20} - \bar{x}_{20} \\ \cdots & \cdots & \cdots \\ x_{N,1} - \bar{x}_1 & \cdots & x_{N,20} - \bar{x}_{20} \end{bmatrix} \tag{8}$$

Multiplying $\mathbf{P}$ by its transpose, $\mathbf{P}'$, yields a quantity which is related to the variance-covariance matrix, $\mathbf{S}$, by the equation

$$\mathbf{P}'\mathbf{P} = (N - \mathbf{I})\mathbf{S} \tag{9}$$

where $\mathbf{I}$ is the identity matrix. By an iterative procedure, a set of orthogonal vectors, $\mathbf{V}_i$ is found such that

$$\mathbf{V}_i\mathbf{P}'\mathbf{P} = \lambda_i\mathbf{V}_i \qquad (i = 1, 2, \ldots, k;\ k \leq 20) \tag{10}$$

where λ_i is the eigenvalue of the ith eigenvector. Equation (10) can be rewritten

$$\mathbf{V}_i(\mathbf{P}'\mathbf{P} - \lambda_i\mathbf{I}) = 0 \tag{11}$$

For $\mathbf{V}_i \neq 0$ we have

$$|\mathbf{P}'\mathbf{P} - \lambda_i\mathbf{I}| = 0 \tag{12}$$

Thus, λ_i is a characteristic root of the $\mathbf{P}'\mathbf{P}$ matrix. From equation (12) the trace of $\mathbf{P}'\mathbf{P}$ is equal to

$$\text{tr } \mathbf{P}'\mathbf{P} = \sum^{20} \lambda_i \tag{13}$$

which is equal to the total variance of the data set. A parameter ℓ_i is related to the trace of $\mathbf{P}'\mathbf{P}$ or the total variance by the equation

$$\ell_i = \frac{\lambda_i}{\text{tr } \mathbf{P}'\mathbf{P}} \tag{14}$$

This parameter is the fractional contribution of the ith eigenvector to the total variance of the data set.

In the iterative procedure, the eigenvector that accounts for the greatest variance is extracted first, and successive vectors have successively smaller variances; that is,

$$\ell_1 > \ell_2 > \ell_3 > \ldots > \ell_i \qquad (15)$$

With this set of eigenvectors, the magnitude of band j of a spectrum from the data set can be reconstructed by the equation

$$x_j = \bar{x}_j + a_1 V_{1,j} + a_2 V_{2,j} + \ldots + a_k V_{k,j} \qquad (16)$$

where a_1, a_2, ..., a_k are scalar multiples of the vectors $\mathbf{V}_i$. The advantage of this procedure is realized when all or most of the total variance can be accounted for by k vectors when $k << 20$. If $k = 2$, then equation (16) becomes

$$x_j = \bar{x}_j + a_1 V_{1,j} + a_2 V_{2,j} \qquad (17)$$

and

$$\ell_1 + \ell_2 = 1.0 \qquad (18)$$

Thus, every spectrum of the data set can be reconstructed from the mean vector and two eigenvectors. In this case, 20 spectral parameters have been reduced to 2 which contain all the spectral information of the data set.

In generating eigenvectors there is no assurance that simple relationships will exist between these vectors and measurable parameters in the ocean. In general the vectors are considered to be abstract components of a k-dimensional vector space from which the original data can be reconstructed. Evidence suggests, however, that close relationships exist for ocean color data.

Vectors From Flight Data

Vector analysis was applied to both the raw MOCS spectra and inflection ratio spectra of line #6A data from the mission on June 24. The latter are presented first. The six most significant vectors derived through vector analysis of the $G_{j,2}$ algorithm are shown in figure 11. The vectors were normalized by the mean vector for comparison with the theoretical data. For this data set, 65.7 percent of the total variance is accounted for by the first vector, and 20.1 percent by the second vector. Each succeeding vector contributes less and less to the variance, as indicated in table III. Comparing the first vector in figure 11(a) with the $H_{j,2}$ spectra in figure 10 shows a clear similarity to the spectrum for patch #2. To duplicate the shape of the $H_{j,2}$ spectrum for patch #1, vectors 1 and 2 have been combined in figure 12 by the equation

$$H_{j,2} = \frac{a_1 V_{1,j} + a_2 V_{2,j}}{\bar{x}_j} \qquad (19)$$

where $a_1 = 1.0$ and $a_2 = 1.3$.

Thus, this data set indicates that the first vector is closely associated with the variation of the suspended matter (algae) in patch #2, whereas for patch #1 both vectors 1 and 2 are needed to explain the variations.

To compare the relative magnitudes of the vectors along the flight path, the a_i coefficients for the first six significant vectors are plotted in figure 13. From table III, these six vectors together account for 99 percent of the total variance. Note the similarity of the AOL data for chlorophyll a and phycoerythrin in figure 6 with the plots of the coefficients for the first two vectors, respectively. The similarity is more easily seen in figure 14 in which the two data sets have been superimposed. The plots suggest an association of the AOL chlorophyll a and phycoerythrin measurements with the first and second vectors, respectively. The correlation coefficients were 0.866 for a_1 and AOL chlorophyll a and 0.912 for a_2 and AOL phycoerythrin.

In an attempt to present a physical interpretation of the first two vectors in figure 11, consider figure 15, adapted from reference 15, showing the absorption spectra of three prominent pigments found in phytoplankton. The spectral ranges covered by the $G_{7,2}$ and $G_{12,2}$ algorithms are also indicated. The $G_{12,2}$ algorithm covers the spectral range of the absorption edge of phycoerythrin. Moreover, for vector 2 in figure 11, the negative feature at band 12 and the positive feature at band 14 seem to monitor this phycoerythrin edge. Similarly, $G_{7,2}$ covers the spectral range of the absorption edge of the carotenoids; this indicates that the negative feature at band 7 for vectors 1 and 2 in figure 11 is monitoring the carotenoids, not chlorophyll a. This is surprising because $G_{7,2}$ has been found to correlate quite well with chlorophyll a, as discussed earlier. There are two factors that must be considered, however, before any such conclusion can be drawn: (1) shifts in the absorption bands between extracted pigments, as in figure 15, and *in vivo* phytoplankton and (2) the much higher percentage of chlorophyll a than carotenoids present in algae cells (ref. 16). Even so, figure 15 does suggest a physical interpretation of the two significant vectors, especially in regard to phycoerythrin. The features in these vectors at bands 12 and 14 account for the major differences in the two spectra in figure 10 for the two phytoplankton patches. As demonstrated in a later paragraph, these differences can sometimes be used for "quick-look" analyses of ocean color data.

The a_3 coefficient for the third vector (fig. 13) also shows a distinct pattern along the track, as opposed to the "noise characteristic" of the remaining 13 vec-

tors. This third vector could be associated with a third parameter in the ocean. However, based on examinations of many data sets, it is suggested that the third vector is a "compensator" for the nonlinear aspect of the spectral variation of the backscattered light as a function of chlorophyll a concentration. Because of this nonlinearity, no one vector can accurately represent the spectral variation over a large change in concentration. Thus, the hypothesis is presented that for the line #6A data set obtained on June 24, the first vector represents the average variation, and the third vector is a second-order correction.

The fourth vector, for which a_4 is plotted in figure 13, could be a "noise" vector. The source of the noise is not known but could fall under several categories: (1) instrument, (2) aircraft motion, (3) atmosphere, or (4) ocean. Most of the remaining vectors probably are either "compensator" or "noise" vectors.

For comparison purposes, vectors were generated from both raw MOCS spectral data and inflection ratio spectra. The raw data vectors and associated coefficients for the line #6A data set are shown in figures 16 and 17. These data give a less clear picture of the important variables within the scene for two major reasons: (1) the raw data are more sensitive to environmental variations, and (2) changes in the raw data are much less linearly related to the spectral features.

Cluster Analysis

Vector analysis has not been performed on the remaining lines of the star pattern flown on June 24. However, with the knowledge from the above analysis, another technique, cluster analysis, was found to be useful for establishing a quick look at the general distribution of patch #1- and patch #2-type species. Consider, first, the cross plot in figure 18 of the a_i coefficients for the first two vectors for the line #6A data set. The pattern in the figure has been divided into and labeled as three clusters of data points. Now consider the inflection ratio spectra in figure 10. These data suggest that for the same value of $H_{7,2}$ (or $G_{7,2}$), there are distinctively different values of $H_{j,2}$ (or $G_{j,2}$) in the upper spectral bands. Thus, if $G_{7,2}$ or an estimate of chlorophyll a based on $G_{7,2}$ through equation (5) is cross plotted with $G_{12,2}$, the two patch-type species should be separable, as shown in figure 19. Similar plots for other lines of the star pattern were used to generate the distribution map in figure 20, where there seems to be a distinct difference in the algal species within and outside the warm core ring. Preliminary *in situ* data (ref. 17) did indicate the presence of a strong algal patch in the ring center (located near the center of the star pattern) which was different from the species outside the warm core ring.

One point needs to be clear: the cluster analysis approach is useful only if distinctly separate clusters appear on plots similar to figure 18. In the general case, clusters overlap and are too close to resolve. Vector analysis, on the other hand, should always yield a more exact result.

Discussion

As previously stated, there is no assurance that characteristic vectors are directly relatable to real parameters in the ocean. On the other hand, there is little doubt that many of the spectral features of visible upwelled light are associated with the absorption and scattering properties of algae. Environmental variations and molecular scattering produce broadband spectral features. The influence of these features is minimized by the inflection ratio algorithm. The remarkable similarities between the inflection ratio spectra of both the theoretical data of the Smith and Baker model and the MOCS data and the normalized vectors leave little doubt of the association of the latter with algae in the ocean. The two prime vectors of the line #6A data set are somehow, perhaps directly, associated with the AOL chlorophyll a and phycoerythrin measurements. It is not certain at this point whether these vectors are associated with entirely different species of algae, but the evidence suggests this possibility. Whereas the AOL technique is used to determine concentrations of two separate pigments, the characteristic vectors generated from MOCS data are associated with all the prominent pigments in the visible spectrum and could, therefore, be species-associated. The interrelationships of the AOL and MOCS data require further study.

One final point of discussion concerns parameters measurable by ocean color. Through laboratory and field experiments, Exton et al. (ref. 18) concluded that through laser fluorosensing techniques "it should be possible to remotely quantify total suspended solids, dissolved organics, attenuation coefficient, chlorophyll a, and phycoerythrin," and Houghton et al. (ref. 19) concluded that "diversity of algae groups can be studied by comparison of chlorophyll and phycoerythrin intensities." Which of these parameters can be determined through passive techniques is still uncertain. The feasibility of chlorophyll a measurements has been established. The results presented in this paper indicate that *in vivo* phycoerythrin has strong enough absorption features that it too can be measured passively. If the other parameters have distinguishable spectral features, they should be measurable through characteristic vectors.

Concluding Remarks

A method combining the characteristic vector analysis approach in conjunction with the inflection ratio algorithm results in a promising technique for remotely separating algal populations having distinctly different spectral signatures. The limit in separating populations depends on the uniqueness of their spectral signatures, their concentrations, and the number of spectral bands comprising the spectra. The technique first uses the inflection ratio algorithm to minimize the broadband variations caused by extraneous parameters and then generates characteristic vectors from the algorithmic data. Vectors generated from raw spectral data are at present difficult to interpret because of the noise and nonlinear aspects of the data. After applying the new technique to data collected during a flight mission on June 24, 1982, the Multichannel Ocean Color Sensor (MOCS) data were found to be in remarkable agreement with the Airborne Oceanographic Lidar (AOL) data, even though the two measurement techniques are quite different. Data from both instruments indicate the presence of two different parameters relatable to algae in and around the warm core ring on June 24. The interrelationship of the data from the two techniques requires further study. Even so, the two instruments flown side-by-side should provide marine scientists with valuable data, real-time or after the event, accompanied by a high level of confidence in the validity of the information. The new technique should be applicable to other remote-sensing data and to any spectral data composed of significant, narrowband signatures mixed with broadband extraneous variations.

NASA Langley Research Center
Hampton, VA 23665
January 16, 1985

References

1. Grew, Gary W.: Real-Time Test of MOCS Algorithm During Superflux 1980. *Chesapeake Bay Plume Study—Superflux 1980.* NASA CP-2188, 1981, pp. 301–322.
2. Grew, Gary W.; and Mayo, Leonard S.: *Ocean Color Algorithm for Remote Sensing of Chlorophyll.* NASA TP-2164, 1983.
3. White, P. G.; Jenkin, K. R.; Ramsey, R. C.; and Sorkin, M.: *Development and Flight Test of the Multichannel Ocean Color Sensor (MOCS).* NASA CR-2311, 1973.
4. Hoge, F. E.; and Swift, R. N.: Application of the NASA Airborne Oceanographic Lidar to the Mapping of Chlorophyll and Other Organic Pigments. *Chesapeake Bay Plume Study—Superflux 1980,* NASA CP-2188, 1981, pp. 349–374.
5. *Warm Core Rings—An Interdisciplinary Study of Warm Core Ring Physics, Chemistry and Biology—Cruise Reports.* Woods Hole Oceanographic Inst., Apr. 1982.
6. *Warm Core Rings—An Interdisciplinary Study of Warm Core Ring Physics, Chemistry and Biology—Cruise Reports.* Woods Hole Oceanographic Inst., June 1982.
7. *Warm Core Rings—An Interdisciplinary Study of Warm Core Ring Physics, Chemistry and Biology—Cruise Reports.* Woods Hole Oceanographic Inst., Aug. 1982.
8. Grew, Gary W.: Characteristic Vector Analysis as a Technique for Signature Extraction of Remote Ocean Color Data. *Remote Sensing of Earth Resources—Volume VI,* F. Shahrokhi, ed., Univ. Tennessee, Space Inst., c.1977, pp. 109–144.
9. Grew, G. W.: Signature Extraction of Ocean Pollutants by Eigenvector Transformation of Remote Spectra. *Conference Proceedings—4th Joint Conference on Sensing of Environmental Pollutants,* American Chem. Soc., c.1978, pp. 659–666.
10. Campbell, Janet W.; and Esaias, Wayne E.: Basis for Spectral Curvature Algorithms in Remote Sensing of Chlorophyll. *Appl. Opt.,* vol. 22, no. 7, Apr. 1983, pp. 1084–1093.
11. Smith, Raymond C.; and Baker, Karen S.: Optical Classification of Natural Waters. *Limnol. & Oceanogr.,* vol. 23, no. 2, Mar. 1978, pp. 260–267.
12. Morrison, Donald F.: *Multivariate Statistical Methods,* Second ed. McGraw-Hill Book Co., c.1976.
13. Anderson, T. W.: *An Introduction to Multivariate Statistical Analysis,* Second ed. John Wiley & Sons, Inc., c.1984.
14. Simonds, J. L.: Application of Characteristic Vector Analysis to Photographic and Optical Response Data. *J. Opt. Soc. America,* vol. 53, no. 8, Aug. 1963, pp. 968–974.
15. Govindjee; and Govindjee, Rajni: The Absorption of Light in Photosynthesis. *Sci. American,* vol. 231, no. 6, Dec. 1974, pp. 68–82.
16. Round, F. E.: *The Biology of the Algae.* St Martin's Press, 1965.
17. Blackwelder, P. L.; Hooker, S. B.; and Olson, D. B.: Radial and Azimuthal Distribution of Warm Core Ring Phytoplankton. *EOS Trans., American Geophys. Union,* vol. 64, no. 52, Dec. 27, 1983, pp. 1082–1083.
18. Exton, R. J.; Houghton, W. M.; Esaias, W.; Harriss, R. C.; Farmer, F. H.; and White, H. H.: Laboratory Analysis of Techniques for Remote Sensing of Estuarine Parameters Using Laser Excitation. *Appl. Opt.,* vol. 22, no. 1, Jan. 1, 1983, pp. 54–64.
19. Houghton, W. M.; Exton, R. J.; and Gregory, R. W.: Field Investigation of Techniques for Remote Laser Sensing of Oceanographic Parameters. *Remote Sensing Environ.,* vol. 13, no. 1, Mar. 1983, pp. 17–32.

TABLE I. MOCS SPECIFICATIONS

Sensor	Image dissector
Scan rate, scans/sec	3.51
No. of spectra per scan	150
Spectral range, nm	400 to 700
Spectral resolution, nm	15
Field of view, deg	17.1
Spatial resolution, mrad	4×2

TABLE II. MOCS SPECTRAL BANDS

Band	Center wavelength, nm
1	400
2	415
3	430
4	445
5	460
6	475
7	490
8	506
9	521
10	537
11	552
12	568
13	584
14	601
15	616
16	631
17	647
18	663
19	678
20	694

TABLE III. VARIANCE OF VECTORS FOR DATA SET FROM JUNE 24, 1982

Vector	Variance, percent	Cumulative variance, percent
1	65.69	65.69
2	20.10	85.79
3	7.67	93.45
4	3.87	97.33
5	1.23	98.55
6	.43	98.99
7	.30	99.29
8	.22	99.51
9	.19	99.70
10	.10	99.79
11	.07	99.86
12	.06	99.92
13	.05	99.97
14	.02	99.99
15	.01	100.00
16	.00	100.00
17	.00	100.00
18	.00	100.00
19	.00	100.00
20	.00	100.00

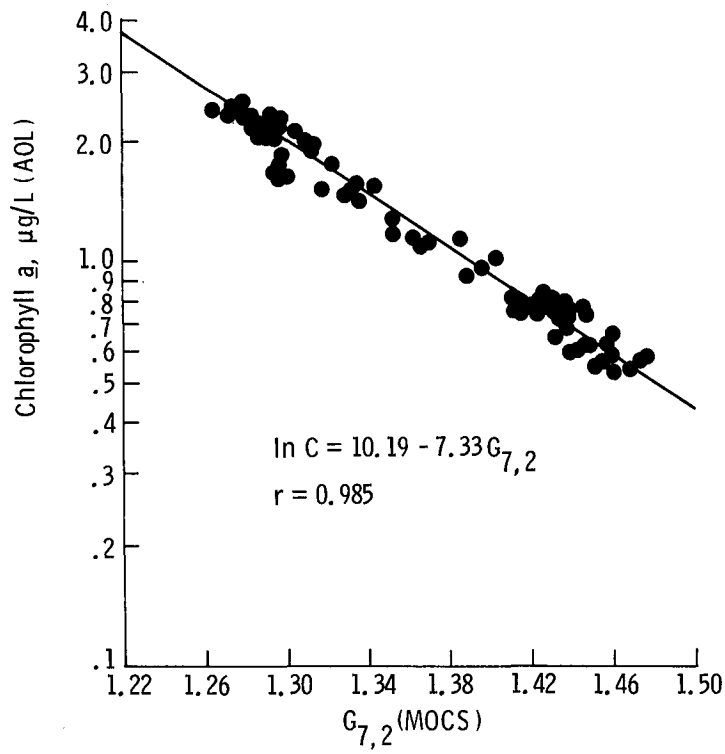

Figure 1. Calibrated AOL chlorophyll a versus $G_{7,2}$ for MOCS data collected at an altitude of 150 m over Nantucket Shoals on May 9, 1981 (ref. 2). The linear regression equation and correlation coefficient are indicated.

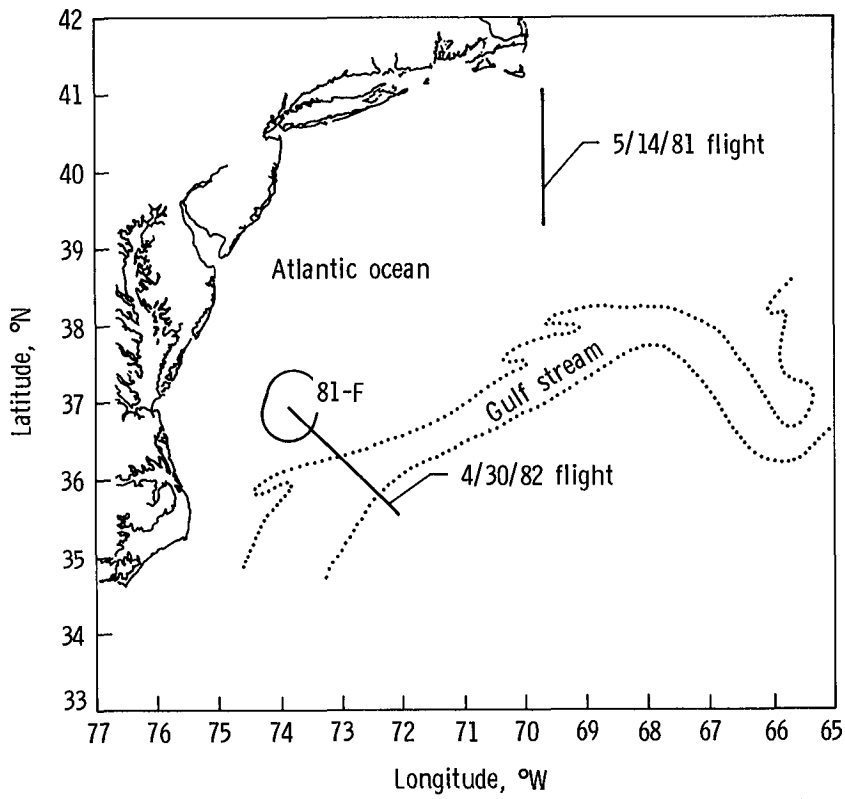

Figure 2. Approximate locations of two AOL/MOCS data collection flight lines.

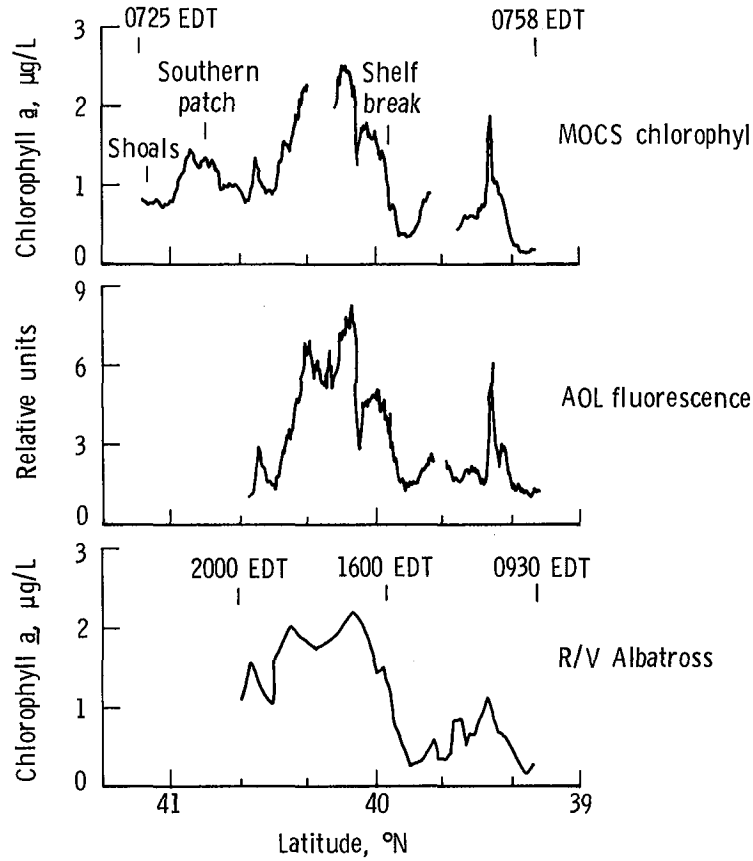

Figure 3. Comparison of chlorophyll *a* concentration measurements made by MOCS and AOL aboard NASA P-3 and by research vessel (R/V) Albatross along longitude 69°40′ W on May 14, 1981. (See fig. 2 and ref. 2.)

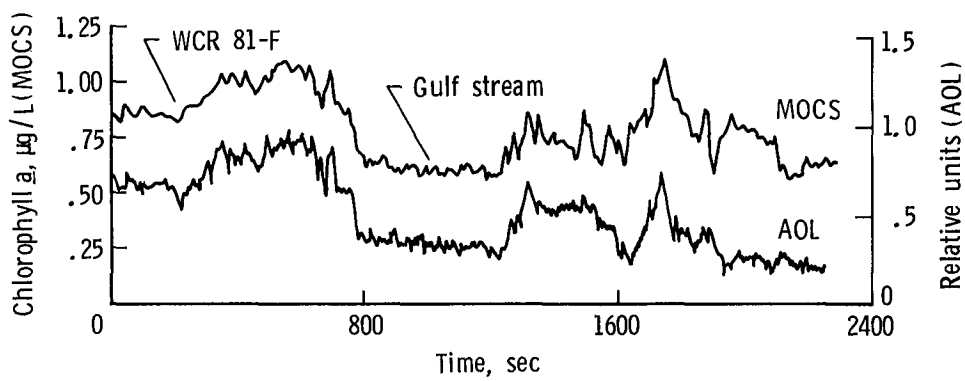

Figure 4. MOCS and AOL data collected along flight line (fig. 2) over warm core ring (WCR) 81-F and Gulf Stream on April 30, 1982.

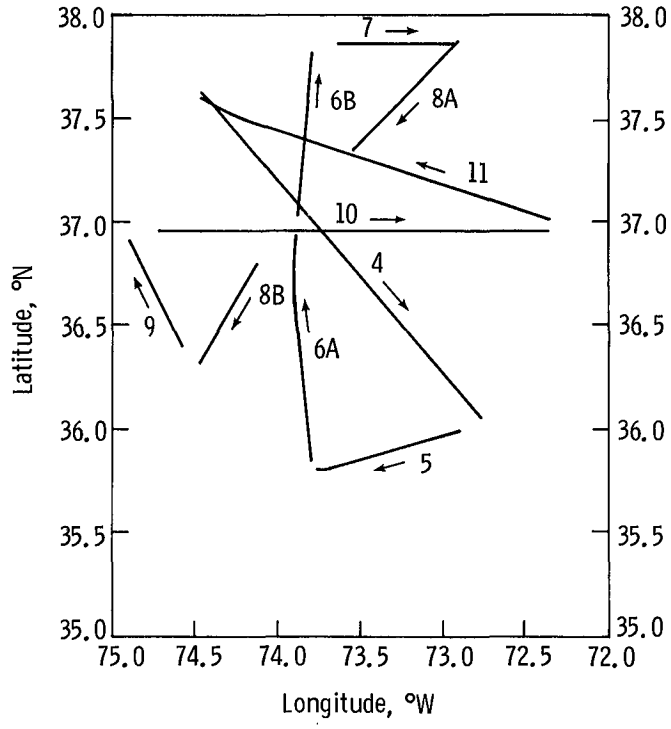

Figure 5. Flight path of NASA P-3 airplane (altitude of 150 m) over warm core ring 82-B on June 24, 1982. Numbers and arrows indicate flight lines and directions.

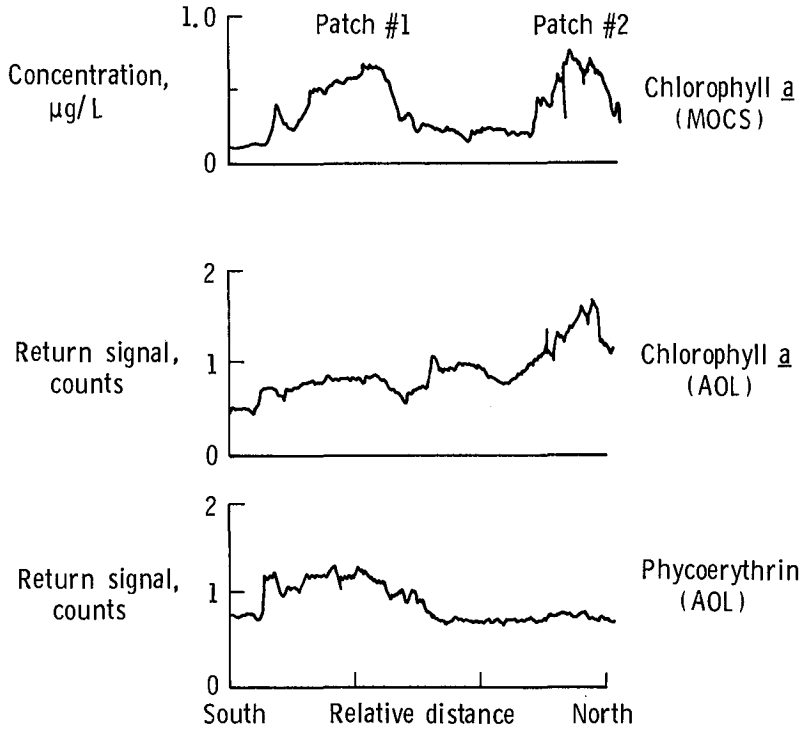

Figure 6. MOCS and AOL data collected along line #6A over warm core ring 82-B on June 24, 1982. For discussion purposes, the two features in the MOCS data have been labeled patch #1 and patch #2.

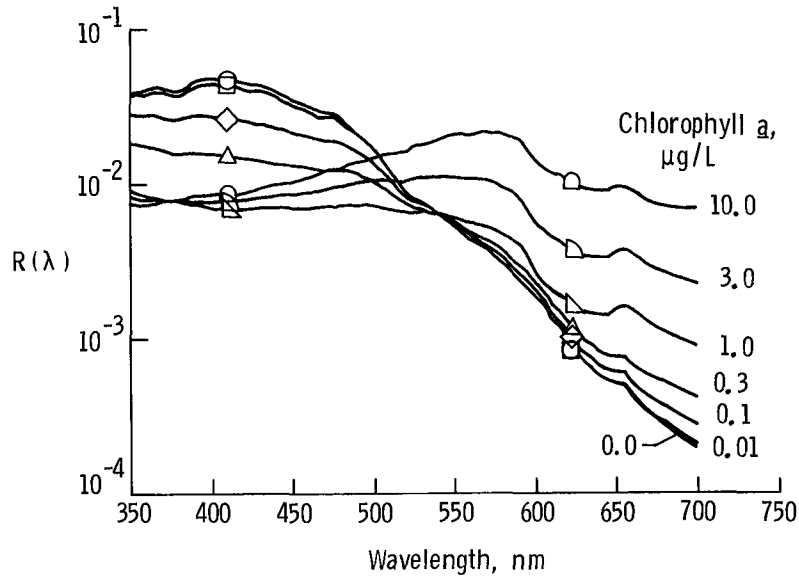

Figure 7. Irradiance reflectance from the ocean generated from Smith and Baker model (ref. 11) as a function of chlorophyll *a* concentration.

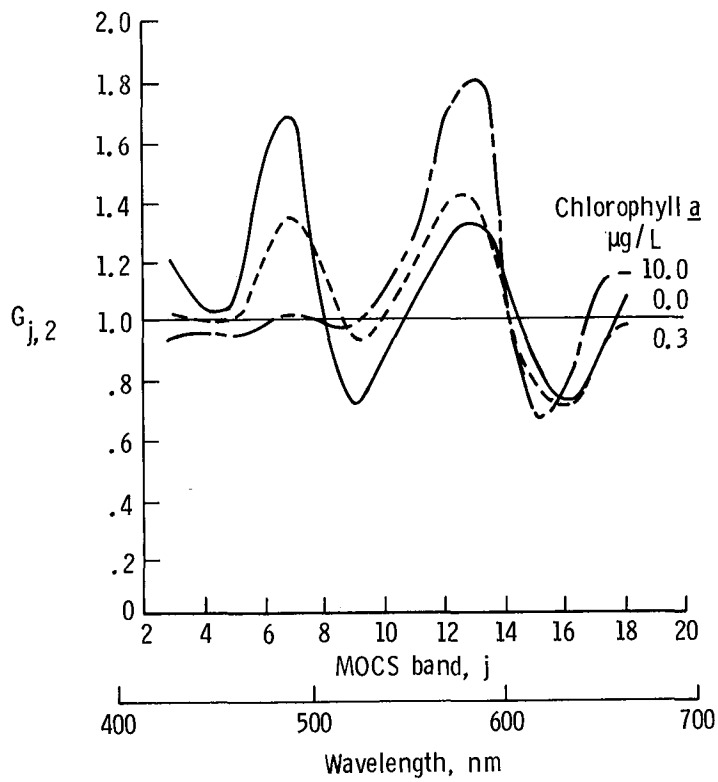

Figure 8. Calculated values of $G_{j,2}$ for three curves in figure 7 from Smith and Baker model.

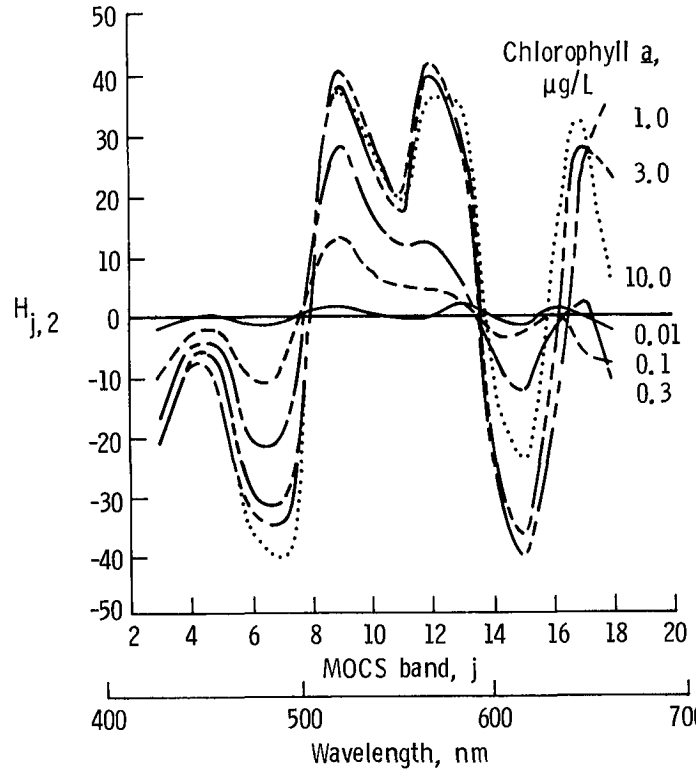

Figure 9. Calculated values of $H_{j,2}$ for Smith and Baker curves in figure 7 (0.0 μg/L curve used for normalization).

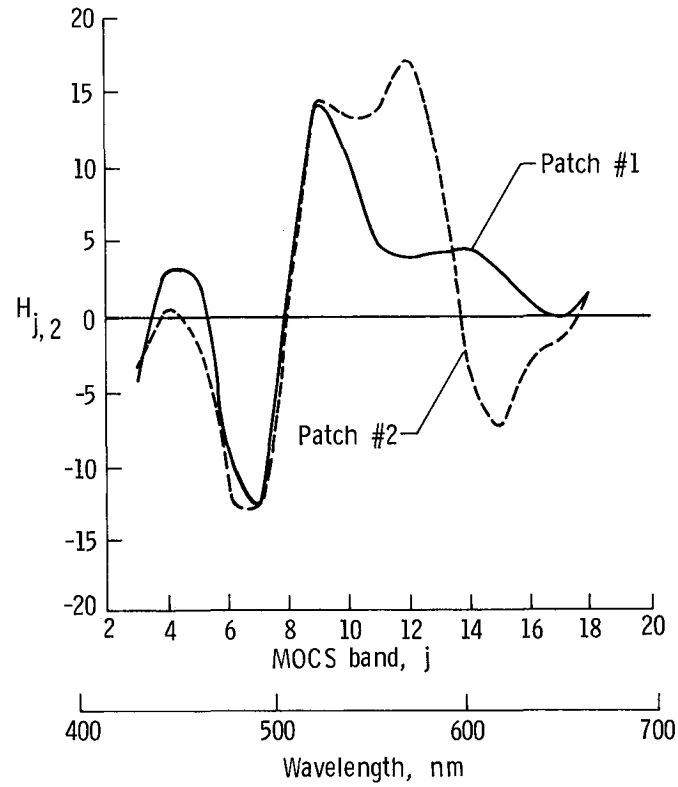

Figure 10. Sample inflection ratio spectra from patch #1 and patch #2.

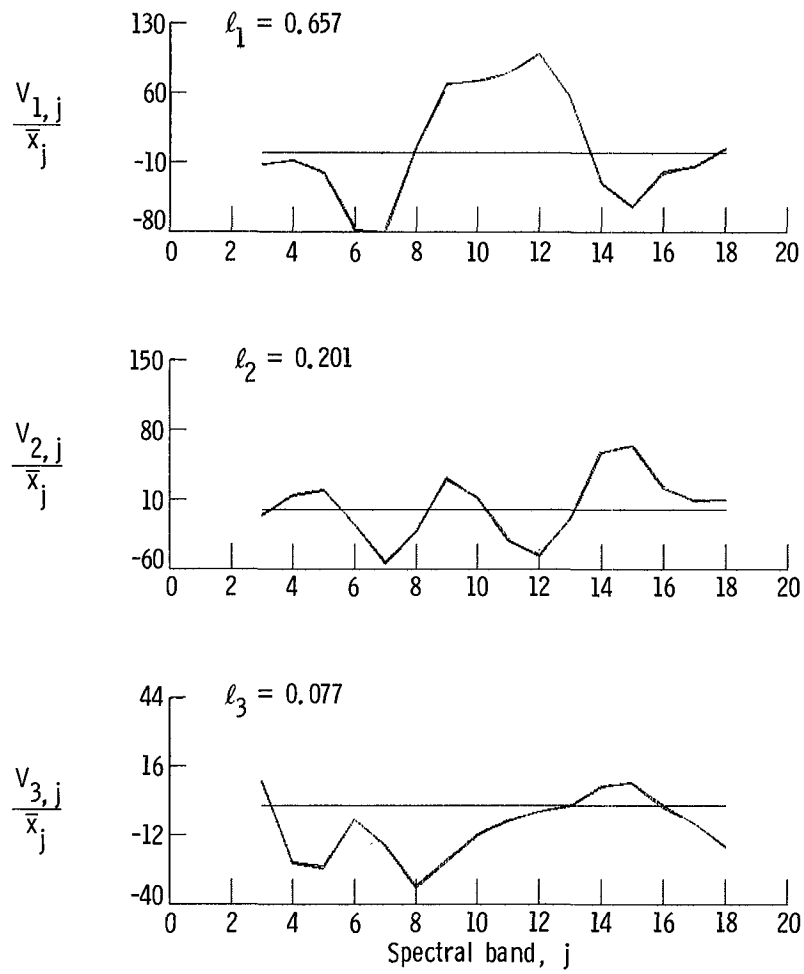

(a) Vectors 1, 2, and 3.

Figure 11. Normalized vectors generated from inflection ratio spectra of MOCS data collected along line #6A on June 24, 1982.

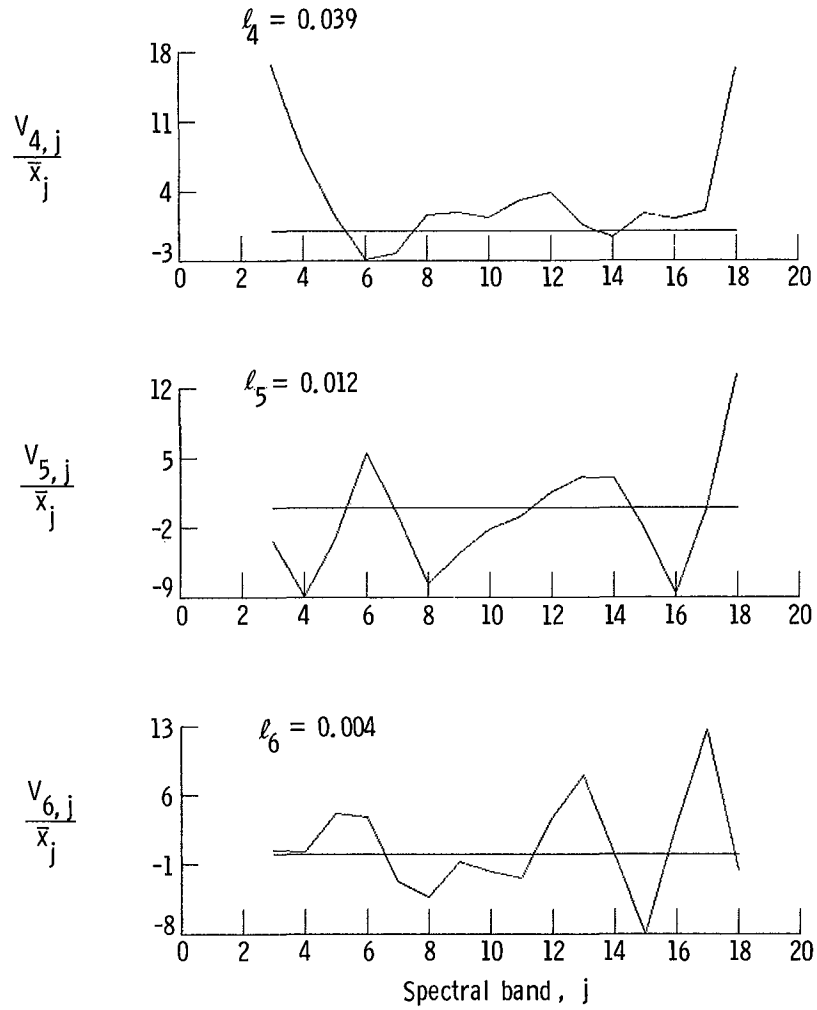

(b) Vectors 4, 5, and 6.

Figure 11. Concluded.

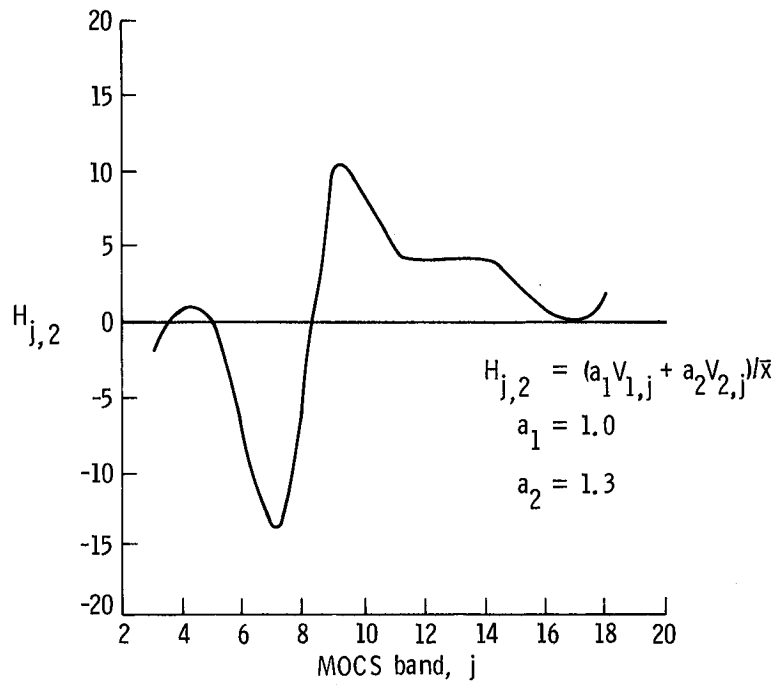

Figure 12. Simulation of $H_{j,2}$ for patch #1 by combining first two significant vectors.

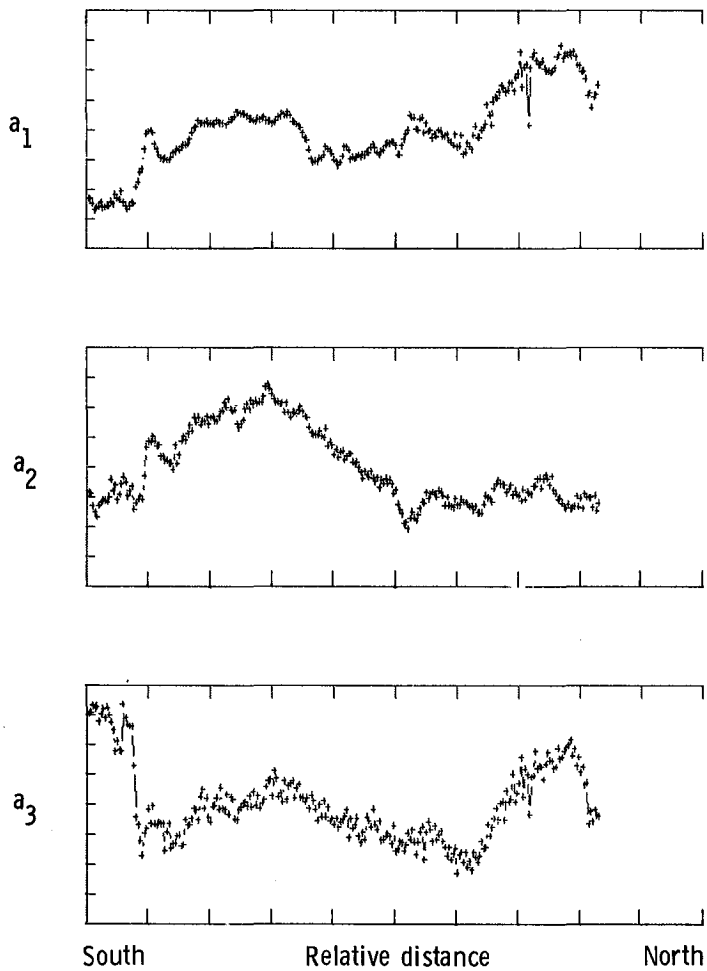

(a) Coefficients for vectors 1, 2, and 3.

Figure 13. Coefficients generated from line #6A data.

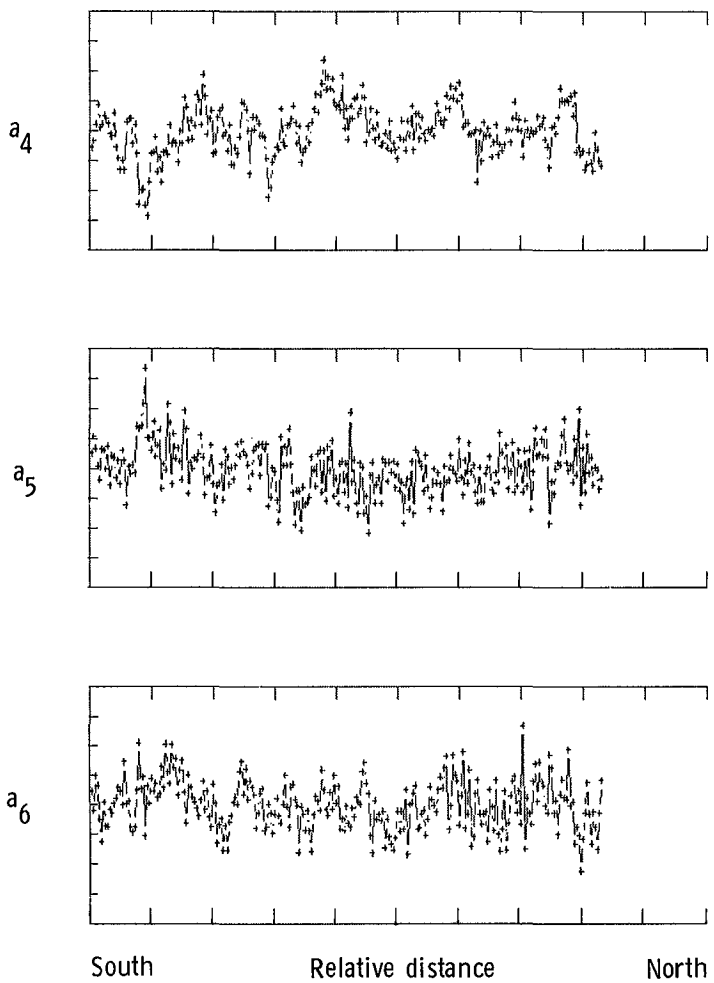

(b) Coefficients for vectors 4, 5, and 6.

Figure 13. Concluded.

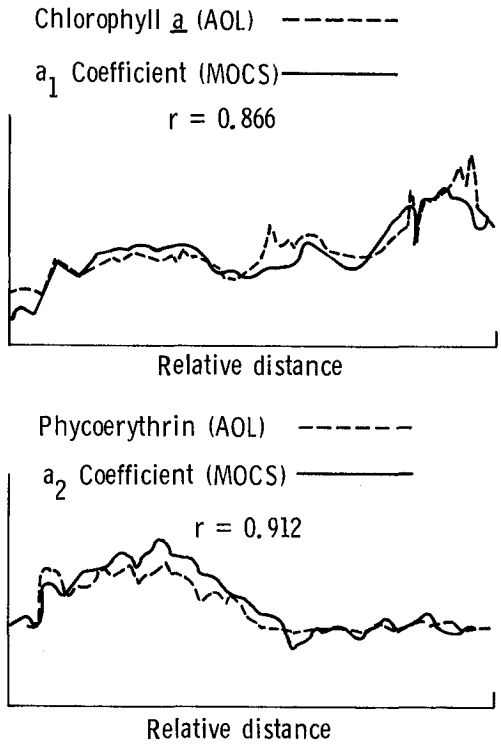

Figure 14. Scaled overlays of AOL data (fig. 6) with a_1 and a_2 coefficients of two most significant vectors generated from MOCS line #6A data (fig. 13). The correlation coefficient, r, is indicated for each overlay.

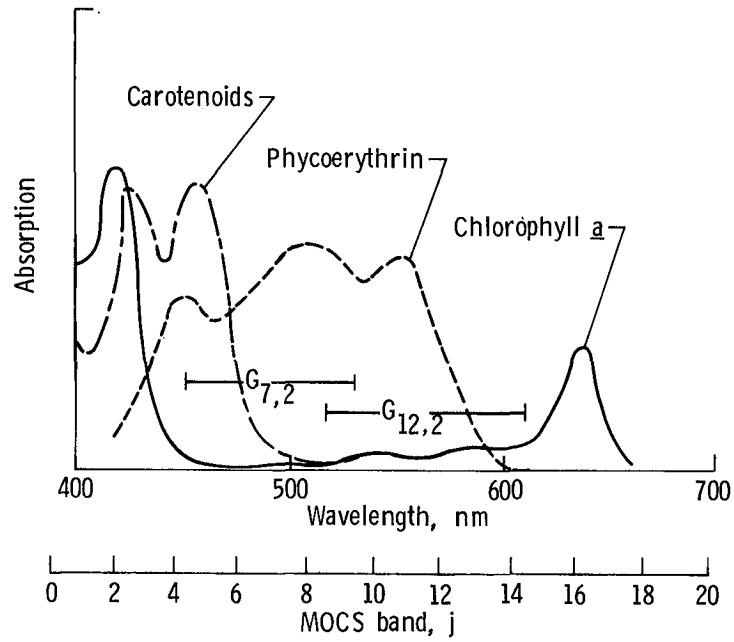

Figure 15. Absorption spectra of three phytopigments (taken from ref. 15). Wavelength ranges of two inflection ratio algorithms, $G_{7,2}$ and $G_{12,2}$, are indicated.

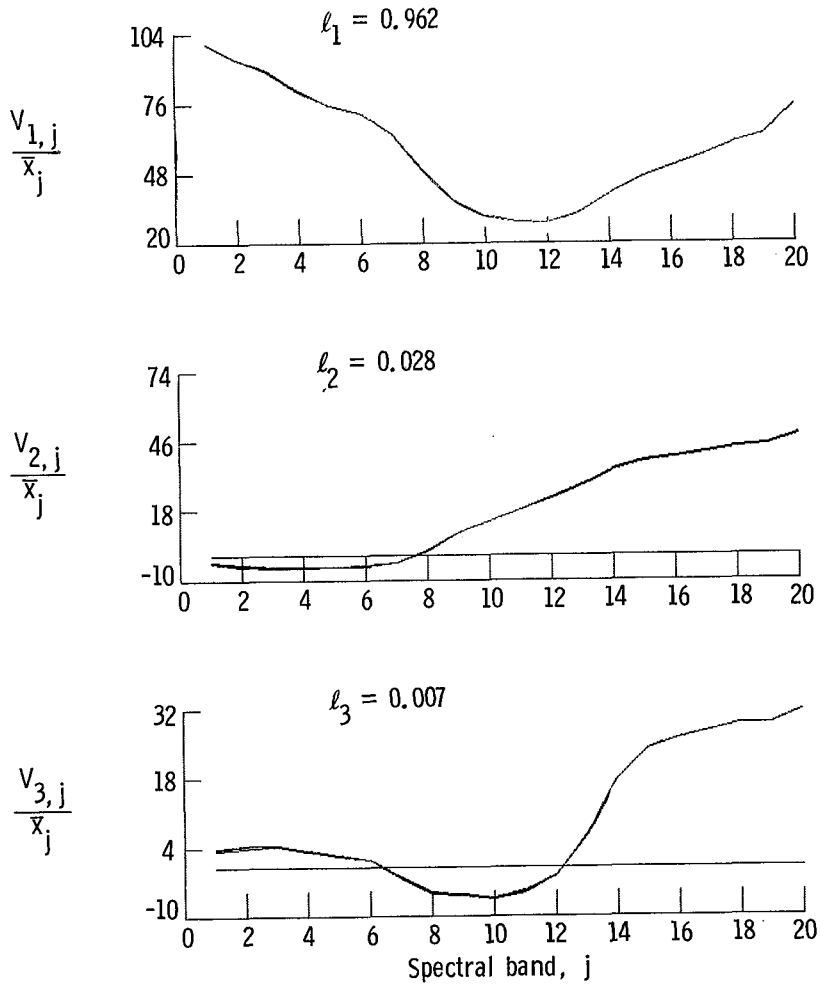

Figure 16. First three normalized vectors generated from raw MOCS data from line #6A. (Compare with fig. 11.)

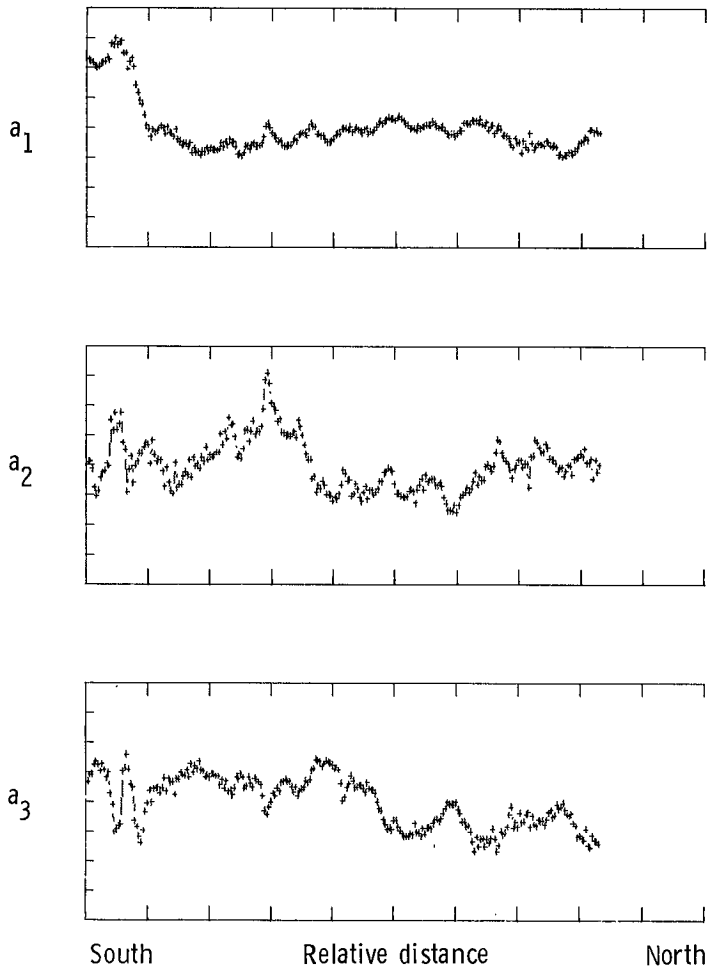

Figure 17. Coefficients for first three vectors generated from raw MOCS data from line #6A. (Compare with fig. 13.)

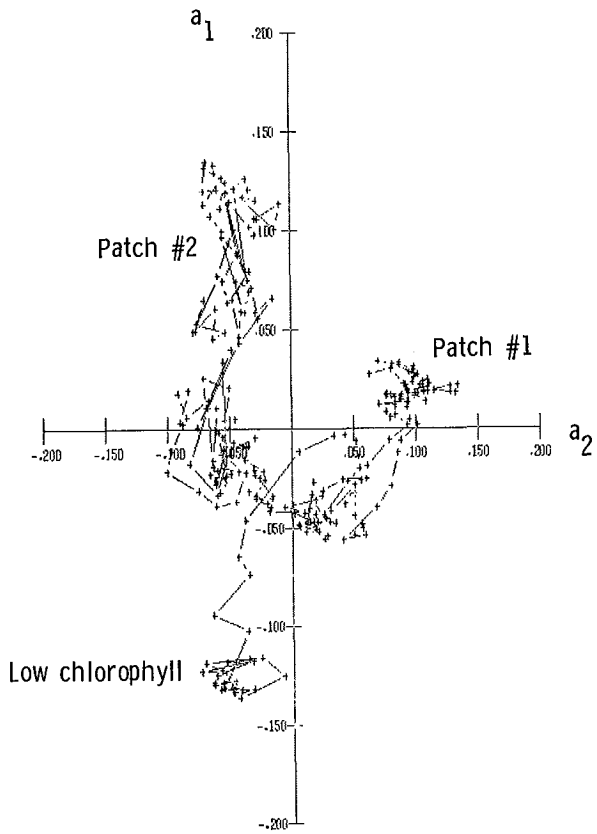

Figure 18. Cross plot of a_1 and a_2 for line #6A. Three clusters of data points are identified.

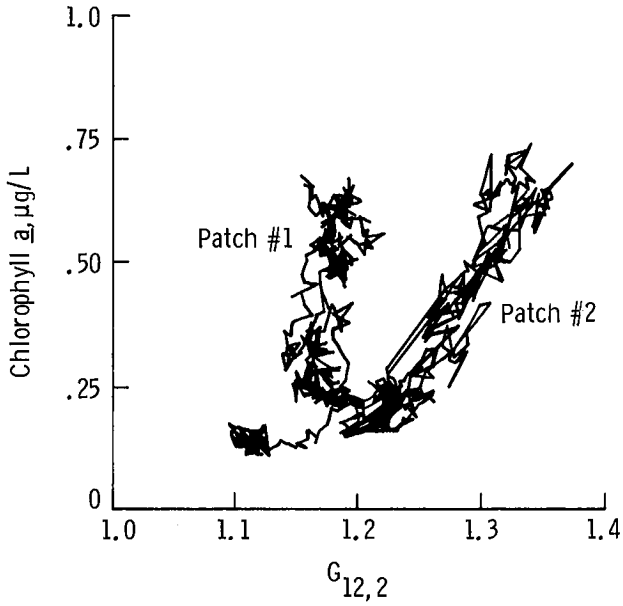

Figure 19. MOCS data from line #6A of estimates of chlorophyll a (eq. (5)) versus MOCS algorithm, $G_{12,2}$. Data from patch #1 and patch #2 are identified.

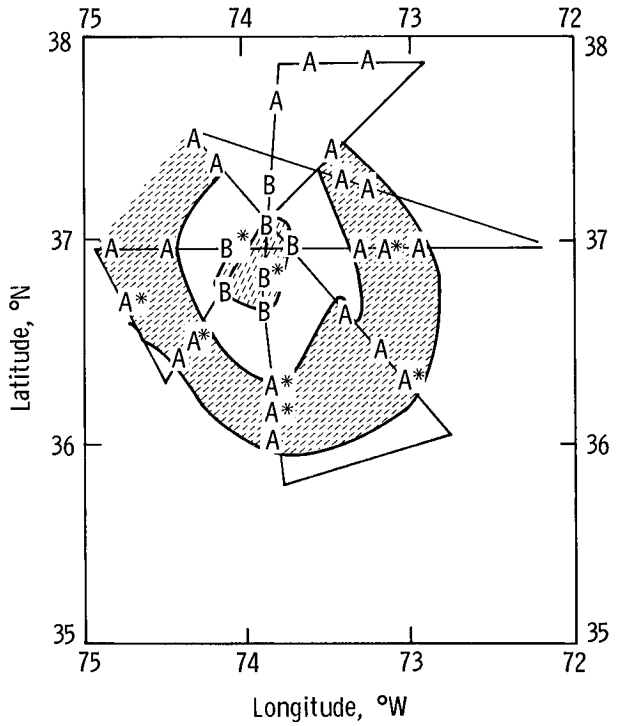

Figure 20. Locations of patch #1 algae (A) and patch #2 algae (B). Highest concentrations are indicated by asterisks.

1. Report No.	2. Government Accession No.	3. Recipient's Catalog No.
NASA TP-2428		

4. Title and Subtitle	5. Report Date
Characteristic Vector Analysis of Inflection Ratio Spectra: New Technique for Analysis of Ocean Color Data	April 1985
	6. Performing Organization Code: 618-32-33-01
7. Author(s): Gary W. Grew	8. Performing Organization Report No.: L-15885
9. Performing Organization Name and Address: NASA Langley Research Center, Hampton, VA 23665	10. Work Unit No.
	11. Contract or Grant No.
12. Sponsoring Agency Name and Address: National Aeronautics and Space Administration, Washington, DC 20546	13. Type of Report and Period Covered: Technical Paper
	14. Sponsoring Agency Code

15. Supplementary Notes

16. Abstract

Characteristic vector analysis applied to inflection ratio spectra is a promising new approach to analyzing spectral data. The technique applied to remote data collected with the Multichannel Ocean Color Sensor (MOCS), a passive sensor, appears to simultaneously map the distribution of two different phytopigments, chlorophyll *a* and phycoerythrin, in the ocean. The data set presented was from a series of warm core ring missions conducted during 1982. The data are shown to compare favorably with a theoretical model and with data collected on the same mission by an active sensor, the Airborne Oceanographic Lidar (AOL).

17. Key Words (Suggested by Authors(s))

Remote sensing
Chlorophyll
Algae
Ocean color
Oceanography
Earth resources

18. Distribution Statement

Unclassified—Unlimited

Subject Category 43

19. Security Classif.(of this report)	20. Security Classif.(of this page)	21. No. of Pages	22. Price
Unclassified	Unclassified	24	A03

For sale by the National Technical Information Service, Springfield, Virginia 22161

NASA-Langley, 1985

National Aeronautics and
Space Administration

Washington, D.C.
20546

Official Business
Penalty for Private Use, $300

THIRD-CLASS BULK RATE

Postage and Fees Paid
National Aeronautics and
Space Administration
NASA-451

NASA

POSTMASTER: If Undeliverable (Section 158 Postal Manual) Do Not Return